PII S0016-7037(02)00881-5

Determination of zircon/melt trace element partition coefficients from SIMS analysis of melt inclusions in zircon

J. B. Thomas,*,[1] R. J. Bodnar,[1] N. Shimizu[2] and A. K. Sinha[1]

[1]Dept. of Geological Sciences, Virginia Tech, Blacksburg, VA 24061, USA
[2]Dept. of Geology and Geophysics, Woods Hole Oceanographic Institution, Woods Hole, MA 02543, USA

Abstract—Partition coefficients ($^{zircon/melt}D_M$) for rare earth elements (REE) (La, Ce, Nd, Sm, Dy, Er and Yb) and other trace elements (Ba, Rb, B, Sr, Ti, Y and Nb) between zircon and melt have been calculated from secondary ion mass spectrometric (SIMS) analyses of zircon/melt inclusion pairs. The melt inclusion-mineral (MIM) technique shows that D_{REE} increase in compatibility with increasing atomic number, similar to results of previous studies. However, D_{REE} determined using the MIM technique are, in general, lower than previously reported values. Calculated D_{REE} indicate that light REE with atomic numbers less than Sm are incompatible in zircon and become more incompatible with decreasing atomic number. This behavior is in contrast to most previously published results which indicate D > 1 and define a flat partitioning pattern for elements from La through Sm. The partition coefficients for the heavy REE determined using the MIM technique are lower than previously published results by factors of ≈15 to 20 but follow a similar trend. These differences are thought to reflect the effects of mineral and/or glass contaminants in samples from earlier studies which employed bulk analysis techniques.

D_{REE} determined using the MIM technique agree well with values predicted using the equations of Brice (1975), which are based on the size and elasticity of crystallographic sites. The presence of Ce^{4+} in the melt results in elevated D_{Ce} compared to neighboring REE due to the similar valence and size of Ce^{4+} and Zr^{4+}. Predicted $^{zircon/melt}D$ values for Ce^{4+} and Ce^{3+} indicate that the Ce^{4+}/Ce^{3+} ratios of the melt ranged from about 10^{-3} to 10^{-2}. Partition coefficients for other trace elements determined in this study increase in compatibility in the order Ba < Rb < B < Sr < Ti < Y < Nb, with Ba, Rb, B and Sr showing incompatible behavior (D_M < 1.0), and Ti, Y and Nb showing compatible behavior (D_M > 1.0).

The effect of partition coefficients on melt evolution during petrogenetic modeling was examined using partition coefficients determined in this study and compared to trends obtained using published partition coefficients. The lower D_{REE} determined in this study result in smaller REE bulk distribution coefficients, for a given mineral assemblage, compared to those calculated using previously reported values. As an example, fractional crystallization of an assemblage composed of 35% hornblende, 64.5% plagioclase and 0.5% zircon produces a melt that becomes increasingly more enriched in Yb using the D_{Yb} from this study. Using D_{Yb} from Fujimaki (1986) results in a melt that becomes progressively depleted in Yb during crystallization. *Copyright © 2002 Elsevier Science Ltd*

1. INTRODUCTION

Accessory minerals in igneous rocks often contain high concentrations of REE and other trace elements (e.g., Arth, 1976; Pearce and Norry, 1979; Brooks et al., 1981; Gromet and Silver, 1983; Mahood and Hildreth, 1983; Irving and Frey, 1984; Fujimaki, 1986; Reed, 1986; Green and Pearson, 1987; Heaman et al., 1990; Maas et al., 1992; Bea et al., 1994; Bea, 1996; Hoskin et al., 2000; O'Hara et al., 2001). Removal of even small quantities of accessory minerals in a fractionating assemblage, or retention of accessory minerals in restites, may strongly affect the trace element concentration of associated melts. For example, Bea (1996) notes that in peraluminous granites 90 to 95% of bulk rock LREE reside within accessories. Bea (1996) further notes that in metaluminous granites amphibole may contain as much as 30 to 35 wt.% of the total HREE, whereas the much less abundant zircon accounts for 30 to 50 wt.% of the HREE. Bea (1996) concludes that major minerals play a very subordinate role with respect to that of

accessories in controlling REE abundances in melts, especially in peraluminous systems. Similarly, Chesner and Ettlinger (1989; see also Sawka et al., 1984) show that removal of as little as 0.052% modal allanite results in depletion of the LREE in the melt by ~50%.

The compositions of melts from which accessory minerals crystallize generally are not well constrained, especially in plutonic rocks. For this reason, inverse modeling using mineral chemistry and partition coefficients has been employed to back-calculate melt compositions (Hinton and Upton, 1991; Guo et al., 1996; Hoskin et al., 2000). Often, workers use the bulk rock as an approximation of the melt composition (e.g., Hoskin et al., 2000). Melt inclusions, such as those described here, provide an opportunity to directly determine the composition of the melt from which the zircon host crystallized. As such, analyses of melt inclusions and their hosts provide information about crystal/melt processes in plutonic (intrusive) magmatic systems that are difficult (or impossible) to assess through conventional methods.

Zircon is ubiquitous in crustal igneous rocks, is highly enriched in HREE, and may exert strong control on the REE evolution of melts from which it crystallizes (Nagasawa, 1970). In some cases,

* Author to whom correspondence should be addressed (jathoma2@vt.edu).

zircon (± apatite) is the only HREE-enriched phase present in granitic rocks. Thus, the accurate determination of trace element partition coefficients for zircon ($^{zircon/melt}D_M$) is important for development and testing of models for melt generation and crystallization. (As this study only involves partitioning of trace elements between melt and host zircon, hereafter $^{zircon/melt}D_M$ is replaced with D_M, where the subscript M refers to the element or elements of interest.) We note that melt inclusions are common in zircon from a wide variety of rock-types including sandstones (detrital zircons), high grade gneisses, syenites, granitoids and basalts (Li, 1994; Chupin et al., 1998; Chesner, 1998).

This paper presents new partitioning data for the REE (La, Ce, Nd, Sm, Dy, Er and Yb) and Ba, Rb, B, Sr, Ti, Y and Nb, obtained from analyses of natural melt inclusions contained in zircon crystals. The melt inclusion-mineral (MIM) technique combines many of the advantages of conventional techniques used previously to determine D_M, while at the same time minimizing or eliminating many of the disadvantages of those techniques. Most previous studies of D_M used bulk analyses of zircon and either coexisting glass or whole rock separates to represent the melt composition (Nagasawa, 1970; Mahood and Hildreth, 1983; Murali et al., 1983; Fujimaki, 1986; Bea et al., 1994). Watson (1980) determined D_{REE} using synthetic zircons grown from peralkaline melts. With the MIM technique, trace element concentrations in melt inclusions and in the immediately adjacent host mineral are measured and used to calculate mineral/melt partition coefficients. Lu et al. (1992) and Sobolev et al. (1996) pioneered this technique to determine partition coefficients in mineral/melt systems. Here, we extend the technique to determine zircon/melt partition coefficients for REE and other trace elements in granitic systems, using crystallized melt inclusions in zircon from the Quottoon Igneous Complex in British Columbia. We emphasize that the geological environment for the zircons studied here is of only secondary importance because the goal of this paper is to describe the feasibility of the MIM technique for determining trace element partitioning between melt and zircon.

2. DESCRIPTION OF THE FIELD AREA

The Quottoon Igneous Complex (QIC) is an elongate, sheet-like body of calc-alkaline tonalite located in northwest British Columbia and southeast Alaska, and is part of the Coast Plutonic Complex (Hutchison, 1982). It is considered to be the southern terminus of the late Cretaceous to Eocene Great Tonalite Sill (Brew and Ford, 1981). Previous studies (Gehrels et al., 1991; Klepeis et al., 1998) have documented that zircon U-Pb ages in the QIC lack an inherited component and that zircons have remained a closed system (for U and Pb) since their formation (~65 to 55 Ma). The QIC stretches over a distance of ≈100 km from the Kowease River at 53°00′N to Pearse Canal near the Canada/United States international border, and is less than 15 km wide. The rocks are tonalitic to quartz dioritic in composition and were emplaced along the Coast shear zone at 4.6 ± 0.6 kb into upper amphibolite facies gneisses of the Central Gneiss Complex (Hutchison, 1982; Crawford et al., 1987). Details of the field relations, petrographic, and geochemical/isotopic data are given by Thomas and Sinha (1999; and references therein) and are briefly summarized below.

On the basis of field and bulk rock data, Thomas and Sinha (1999) divided the Quottoon rocks into two distinct suites. Suite I rocks contain abundant reacted mafic enclaves and are interpreted to have evolved dominantly by magma mixing and assimilation/fractional crystallization processes. The Suite II rocks are more homogeneous, contain fewer mafic enclaves, and evolved dominantly by assimilation and fractional crystallization processes. Mafic and felsic dikes occur in both suites and are interpreted as late stage features based on crosscutting relationships.

3. METHODOLOGY

3.1. Mineral and Melt Inclusion Petrography

The zircons studied here were extracted from sample 2093 (Thomas and Sinha, 1999), a coarse-grained hornblende-biotite quartz diorite from Suite I of the QIC. Accessory minerals include ilmenite, magnetite, apatite and zircon. Zircons have length:width ratios ranging from 2:1 to 10:1, are typically euhedral and clear, and contain both melt and solid inclusions. Zircon occurs as inclusions in early crystallizing plagioclase and hornblende, as well as in later crystallizing biotite and quartz, indicating that zircon was forming early in the crystallization history, and may have continued to crystallize into the later stages of crystallization of the QIC.

Zircon crystals containing melt inclusions range from 500 to 1000 μm in maximum dimension. Melt inclusions in the zircons are primary and randomly distributed in the crystals (Roedder, 1984) with sizes ranging from <10 μm to >100 μm. The average size of studied inclusions is ≈25 to 50 μm because larger inclusions in the crystals tended to decrepitate during the homogenization process. Melt inclusion morphologies range from rounded to elongate to negative-crystal forms. Some melt inclusions are intersected by cracks but all of the inclusions studied occur in crack-free zones. Most melt inclusions do not contain recognizable bubbles and all melt inclusions are crystalline at room temperature (Fig. 1a). Before heating, all of the melt inclusions contained fine-grained aggregates of mostly quartz and feldspar (based on petrographic and electron microprobe analyses of unheated inclusions which were open to the surface) causing the inclusions to appear dark in color. Water that exsolved from the melt occurs as films and distorted bubbles within the crystallized inclusions (Yang and Bodnar, 1994; Lowenstern, 1995; Thomas and Webster, 2000).

3.2. Analytical Techniques

Zircons were separated by conventional techniques and examined under a petrographic microscope to identify crystals containing melt inclusions. Only inclusions near the cores of crystals (i.e., away from the crystal edges) and away from fractures were selected. All of the melt inclusions were partially to completely crystallized, due to slow cooling following entrapment in a plutonic environment. A zircon containing a crystallized (as found) melt inclusion is shown in Figure 1a; a back scattered electron image of the same inclusion after homogenization and exposure at the surface is shown in Fig. 1b.

Selected zircons containing melt inclusions were heated under pressure (1200 to 1600 bars in argon) in a TZM vessel to homogenize the melt inclusions and produce a homogeneous
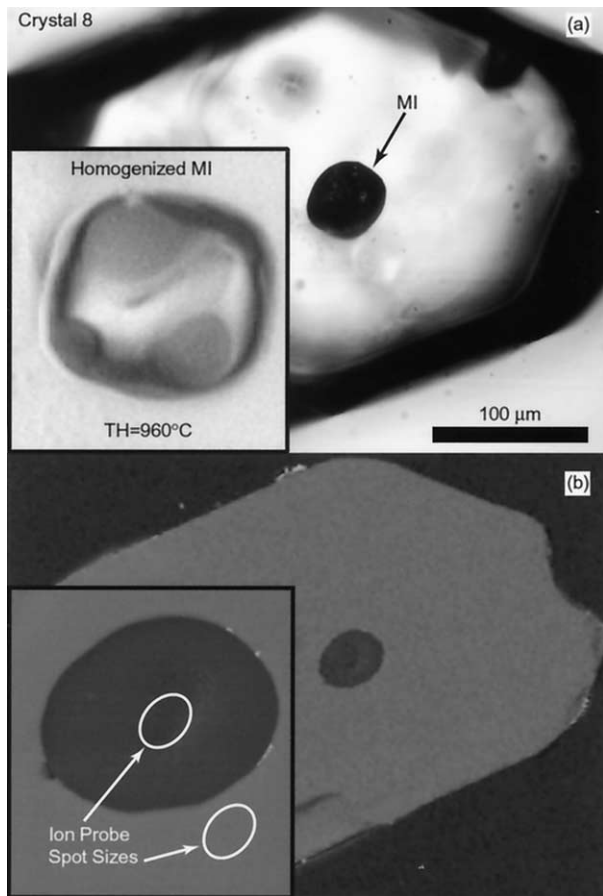
Fig. 1. Melt inclusion in zircon crystal #8 (Table 1). (a) Transmitted light photograph of a zircon containing an unhomogenized (as found) melt inclusion (MI). Inset shows an enlargement of the same inclusion after homogenization. (b) Back-scattered electron image of the same zircon containing the homogenized melt inclusion exposed at the surface by polishing. Inset shows enlargement of the same inclusion along with representative ion probe spot sizes.

glass. Previous workers (Thomas, 1994a, 1994b; Schmidt et al., 1998; Student and Bodnar, 1996, 1999) have shown that heating inclusions under pressure minimizes decrepitation of the inclusions during homogenization, compared to heating at one atmosphere. Note that the internal pressure in the melt inclusions at homogenization is most likely higher than the confining pressure during the experiment (Student and Bodnar, 1996). Starting at 750°C, the inclusions were heated in approximately 20°C increments to determine the homogenization temperature. After each increment of heating, the inclusions were quenched and examined to determine the degree of homogeneity. If an inclusion had not completely homogenized, the sample was placed back into the pressure vessel and heated to a temperature ≈20° higher than the previous step. This process was repeated until complete homogenization was achieved. One inclusion (#B2, Table 1) was heated in a single step to 1000°C and quenched. Previous workers (Sobolev et al., 1990) noted that long duration heating experiments on melt inclusions in other minerals (olivine, plagioclase and clinopyroxene) can result in loss of hydrogen, effectively changing both the water content and oxidation state of the melt. Results presented below suggest

that melt inclusions in zircon studied here have not been similarly affected during the homogenization process.

Zircons containing homogenized melt inclusions were mounted in epoxy and polished to expose the glass inclusion at the surface. Major and minor element compositions (Si, Ti, Al, Mg, Ca, Mn, Fe, Na, K, P, F, Cl, Table 1) of the melt inclusions were determined at Virginia Tech with a Caméca® SX-50 electron microprobe equipped with four wavelength-dispersive spectrometers enabling four elements to be measured simultaneously. For glass (melt inclusion) analyses, an accelerating voltage of 15 kV was used with a beam current of 2 nA, and a beam diameter $< 5\mu$m. Na and K were measured in the first 30 s to minimize the effect of volatization. For electron microprobe analyses of zircon (Table 2) the beam current was increased to 100 nA with a beam diameter of $\sim 1\mu$m. Analytical schemes for melt inclusions and zircons used 20 to 40 s counting times for major elements; for minor and trace elements the counting times were 60 to 600 s. Initial standardization was performed with a combination of minerals and glasses similar in composition to the melt inclusions and the host zircons. The accuracy of major element data is better than ±2% relative, and the accuracy of minor element analyses varies from 2 to 10% relative.

Trace element abundances were measured with a Caméca® IMS 3f ion microprobe at Woods Hole Oceanographic Institute using previously described procedures (e.g., Shimizu and Hart, 1982; Shimizu et al., 1997; Shimizu, 1998). One analytical scheme was used for REE, and a different protocol was used for the other trace elements (Ba, Rb, B, Sr, Ti, Y, Nb). Gold-coated polished sections were analyzed using a primary O^- beam with a primary beam current of ~ 1 nA. A beam diameter of ~ 12 to 15 μm was used for REE analyses; for other trace elements an ~ 8 to 10 μm diameter beam was used. A larger beam diameter was required for REE analyses owing to the lower ion yield for these elements compared to the other trace elements analyzed. Molecular ion interferences were suppressed by offsetting the secondary-ion accelerating voltage by 60 V for REE (and 90 V for other trace elements) with an energy window of ±10 V using an energy-filtering technique (Shimizu and Hart, 1982). Element abundances were determined by converting secondary-ion intensity (ratioed against silicon), using empirical relationships between intensity and concentration based on analyses of rhyolite glass standards. Analytical uncertainties are mainly due to counting statistics; in the present study they are 5 to 15% for the REE and 3 to 8% for the other trace elements.

Fourteen zircons, each containing a single homogenized melt inclusion, were analyzed by electron microprobe (EPMA) and SIMS (Table 1). Zircon compositions obtained from EPMA and SIMS are listed in Table 2. EPMA totals for the homogenized melt inclusions range from 90.8 to 96.12. Differences from 100% are predominantly due to water (or other volatiles) in the glass (Devine et al., 1995). Water contents of melt inclusions were not determined by SIMS because such an analysis requires a different analytical scheme than that used for trace elements and multiple analyses of individual inclusions were not always possible, due to the small size of the melt inclusions. For those inclusions that were large enough for multiple analyses, duplicate trace element analyses were conducted rather than water analyses. Zircon was analyzed immediately adjacent to the melt inclusions. Cathodoluminescence

J. B. Thomas, R. J.Bodnar, N.Shimuzu, and A. K.Sinha

Table 1. Major oxides and trace element concentrations from melt inclusions.

	#1	#1-1	#B1	#B2	#4	#7	#1-11	#35	#46	#I	#G	#8	#9	#16
SiO_2 (wt. %)	78.55	78.88	76.67	77.91	77.8	76.99	75.88	76.20	75.96	78.12	77.47	79.4	79.25	76.63
TiO_2	0.04	n.d.	0.18	0.24	0.08	0.18	0.06	0.31	0.38	0.25	0.10	0.45	n.d.	0.48
Al_2O_3	12.47	12.93	13.94	12.21	13.63	12.91	12.87	13.20	13.67	12.4	13.03	11.95	12.88	12.38
MgO	0.06	0.03	0.07	0.02	0.01	0.02	n.d.	0.08	0.08	0.05	0.02	0.03	0.02	0.13
CaO	0.59	0.66	1.07	0.50	1.00	0.97	0.66	0.68	0.80	0.83	0.97	0.97	0.75	1.19
MnO	n.d.	0.03	0.04	n.d.	0.01	0.01	0.03	0.17	0.03	0.01	0.06	n.d.	0.04	0.02
FeO_t	0.49	0.48	0.87	0.64	0.32	0.59	0.46	0.43	0.81	0.21	0.29	0.54	0.45	0.97
Na_2O	2.26	1.29	2.11	2.6	2.32	3.02	5.23	2.84	2.86	2.53	2.78	2.55	1.36	3.62
K_2O	5.47	5.58	4.98	5.83	4.8	5.31	4.71	6.05	5.38	5.56	5.21	4.11	5.23	4.53
P_2O_5	0.06	0.06	0.06	0.05	0.03	n.d.	n.d.	0.04	0.03	0.03	0.06	n.d.	0.02	0.04
F	0.44	—	—	0.17	0.30	—	—	—	0.19	—	—	—	—	0.84
Cl	0.05	0.04	0.17	0.14	0.06	0.13	0.05	0.00	0.15	0.18	0.16	0.20	0.11	0.11
Total (norm. to 100%)	100	100	100	100	100	100	100	100	100	100	100	100	100	100
Total (measured)	94.92	92.56	94.28	96.12	94.13	95.14	90.80	93.46	91.42	90.85	92.50	91.96	91.68	94.21
Ba (ppm)	—	—	—	—	—	—	—	—	—	—	—	1646	640	1879
Rb	—	—	—	—	—	—	—	—	—	—	—	150	138	166
B	—	—	—	—	—	—	—	—	—	—	—	83.8	137	71.2
Sr	—	—	—	—	—	—	—	—	—	—	—	191	81.3	193
Ti	—	—	—	—	—	—	—	—	—	—	—	1966	350	1748
Y	—	—	—	—	—	—	—	—	—	—	—	17.1	5.94	345
Nb	—	—	—	—	—	—	—	—	—	—	—	11.1	6.03	16.8
La	20.9	22.8	38.5	19.4	96.6	20.1	31.9	30.4	31	13.6	16.9	—	—	—
Ce	34.4	41.4	76.8	39.2	133	36.3	56.7	53.8	55.5	25.3	32	—	—	—
Nd	9.96	12.6	28.1	11	37	13	16.3	20	22.6	6.79	8.37	—	—	—
Sm	1.55	2.04	5.58	1.91	6.06	1.67	3.19	3.23	3.47	0.29	1.62	—	—	—
Dy	3.35	3.30	8.98	6.35	18.8	1.98	13.6	3.06	3.35	1.58	1.29	—	—	—
Er	5.36	3.88	9.91	9.21	34.9	2.33	21.8	4.04	2.17	2.15	0.79	—	—	—
Yb	13	6.13	13.8	15.9	83.4	4.38	33.7	7.46	3.15	7.64	1.50	—	—	—
Ce/Ce*	1.26	1.28	1.23	1.41	1.13	1.18	1.31	1.15	1.1	1.39	1.42			
La_N/Yb_N	1.07	2.49	1.87	0.82	0.78	3.07	0.63	2.72	6.59	1.19	7.51			
Zr	881	207	327	348	939	728	713	70.2	390	508	649	167[d]	553[e]	1063[f]
ZST (°C)[a]	984	844	881	869	999	943	912	725	885	908	937	809	949	974
TH (°C)[b]	960	925	875	1000[c]	960	960	960	785	992	950	950	960	960	960

Dashes = not analyzed; n.d. = not detected.

FeO_t = FeO + Fe_2O_3.

Ce/Ce* = $Ce_N/\sqrt{(La_N \times Nd_N)}$; Chondrite normalization values of Nakamura, 1974.

[a] ZST = zircon saturation temperature (Watson and Harrison, 1983).

[b] TH = total homogenization temperature.

[c] Heated to 1000°C in one step, TH less than this value.

Zr = Zr measured by electron microprobe.

Zr from SIMS; [d] = 234 ppm; [e] = 431 ppm; [f] = 1001 ppm.

imaging of the zircons, back scattered electron imaging of melt inclusions and host zircons, and trace element EPMA traverses across melt inclusions and adjacent host zircon reveal no significant zoning of the host zircon in the immediate vicinity of the melt inclusion (Figs. 1 to 3).

As noted above, water contents of melt inclusions were estimated from EPMA data assuming that differences from 100% totals are due to water or other volatile elements. Anderson (1974) and Yang and Bodnar (1994) used this technique to determine water contnets of melt inclusions, and Devine et al. (1995) compared water contents of glasses determined by SIMS, FTIR and EPMA, and found that EPMA difference values provide acceptable estimates of H_2O contents as long as the water content is above 1 wt.%. Applying the difference technique to our melt inclusions suggests volatile contents from 4 to perhaps as high as 9 wt.% H_2O. As observed by numerous workers, the water in crystallized melt inclusions occurs as thin films and/or one or more distorted vapor bubbles within the crystalline mass (Skirius et al., 1990; Lowenstern 1995; Yang and Bodnar, 1994; Thomas and Webster, 2000). High water

contents are not unusual or unexpected in melt inclusions from deep intrusive systems such as the QIC. Thus, Yang and Bodnar (1994) found water contents up to 4.2 wt.% in melt inclusions in granodiorites, Lowenstern (1994) found water contents up to 8 wt.% in melt inclusions from the Pine Grove system, and Thomas and Webster (2000) report water contents as high as 11 wt. % in crystallized melt inclusions from pegmatites. That the inclusions in this study maintain these high water contents during homogenization and quenching is also consistent with results of previous studies. Thus, Skirius et al. (1990) note that *"few or no volatiles leak from inclusions during heating,"* and Lowenstern and Mahood (1991) showed that crystallized melt inclusions were *more* likely to retain the original water content compared to glassy inclusions.

4. RESULTS

Results of heating experiments to homogenize melt inclusions are listed in Table 1. Twelve of the fourteen melt inclusions homogenized between 925° and 1000°C, with one at

Table 2. Major oxides and trace element concentrations of zircon hosts. Major oxides were not determined for #G and #I.

	#1	#1-1	#B1	#B2	#4	#7	#1-11	#35	#46	#I	#G	#8	#9	#16
SiO_2 (wt. %)	31.26	31.46	31.31	31.22	31.50	31.36	31.52	30.89	31.15	—	—	31.54	31.98	31.37
TiO_2	n.d.	n.d.	0.01	0.01	n.d.	n.d.	0.01	0.01	n.d.	—	—	n.d.	n.s.	0.01
Al_2O_3	0.01	0.03	0.01	n.d.	n.d.	n.d.	0.01	0.01	0.02	—	—	0.01	0.01	n.d.
FeO_t	n.d.	n.d.	n.d.	n.d.	0.01	n.d.	n.d.	n.d.	n.d.	—	—	n.d.	n.d.	n.d.
MnO	n.d.	n.d.	n.d.	n.d.	0.01	0.01	n.d.	n.d.	n.d.	—	—	0.01	n.d.	n.d.
MgO	n.d.	n.d.	n.d.	n.d.	0.01	n.d.	n.d.	n.d.	n.d.	—	—	n.d.	n.d.	n.d.
CaO	n.d.	0.01	0.01	0.01	0.01	n.d.	n.d.	n.d.	0.02	—	—	n.d.	n.d.	0.01
K_2O	n.d.	n.d.	n.d.	n.d.	n.d.	n.d.	0.01	0.01	0.01	—	—	0.01	0.01	0.03
P_2O_5	n.d.	n.d.	n.d.	n.d.	n.d.	n.d.	n.d.	n.d.	n.d.	—	—	n.d.	n.d.	n.d.
Y_2O_3	0.04	0.05	0.04	0.16	0.04	0.05	0.05	0.12	0.02	—	—	0.03	0.01	0.06
ZrO_2	66.59	66.59	66.49	66.71	67.27	66.85	65.99	66.61	66.80	—	—	66.68	66.68	67.14
HfO_2	0.68	0.74	0.58	0.58	0.78	0.77	0.69	0.81	0.71	—	—	1.05	1.18	0.97
Total	98.59	98.88	98.45	98.70	99.62	99.04	98.28	98.45	98.72	—	—	99.32	99.89	99.59
Ba (ppm)	—	—	—	—	—	—	—	—	—	—	—	4.94	3.20	7.52
Rb	—	—	—	—	—	—	—	—	—	—	—	1.20	0.83	0.66
B	—	—	—	—	—	—	—	—	—	—	—	1.59	1.92	1.21
Sr	—	—	—	—	—	—	—	—	—	—	—	6.49	3.5	2.7
Ti	—	—	—	—	—	—	—	—	—	—	—	6496	5891	5508
Y	—	—	—	—	—	—	—	—	—	—	—	860	1135	825
Nb	—	—	—	—	—	—	—	—	—	—	—	3454	1424	3442
La	1.04	0.91	2.69	4.27	2.9	0.4	1.92	7.89	0.62	0.41	0.84	—	—	—
Ce	70.8	34.4	112	38.8	186	22.1	52.7	67.8	23.9	27.9	24	—	—	—
Nd	15.7	2.53	14	5.84	30.8	1.43	9.14	16.2	7.91	2.1	1.34	—	—	—
Sm	18	5.51	19.9	7.91	30.4	4.16	14.6	10.5	2.6	3.26	2.06	—	—	—
Dy	245	66.3	202	107	365	72.4	168	159	64.7	82.7	34.1	—	—	—
Er	388	113	291	194	625	137	284	303	114	131	55.3	—	—	—
Yb	670	249	494	348	1170	290	439	569	259	268	145	—	—	—
Ce/Ce*	9.2	11.9	9.61	4.09	10.4	15.4	6.63	3.16	5.67	15.8	11.9	—	—	—
La_N/Yb_N	0.00104	0.00245	0.00365	0.00820	0.00166	0.00093	0.00292	0.00927	0.00160	0.00101	0.00388	—	—	—

Abbreviations and symbols are the same as in Table 1.

875°C and one at 785°C. One melt inclusion (#B2) was homogenized by heating to 1000°C in a single step. Therefore, the actual homogenization temperature (TH) of this one inclusion is somewhat less than 1000°C. However, as the majority of the inclusions have homogenization temperatures in the range 950 to 1000°C (Table 1), the reported TH of inclusion #B2 (1000°C) is probably only a few tens of degrees higher than the actual temperature.

The goal of the heating experiments was to produce a homogeneous glass for subsequent electron and ion probe analyses, and no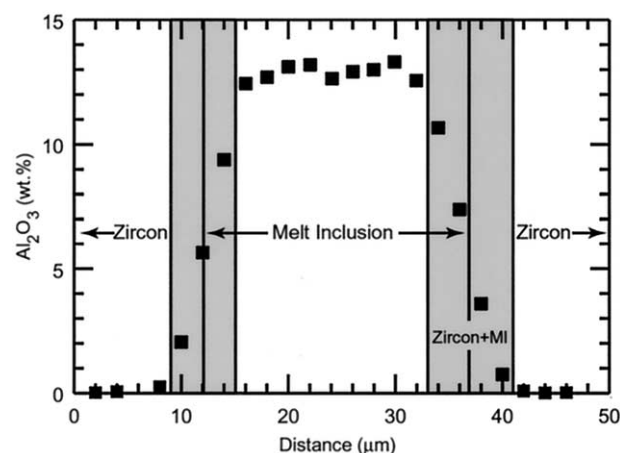t to determine the TH. However, if these analytical data are to be used to calculate partition coefficients, it is imperative that the melt and the host be in chemical equilibrium. If the melt and the host are in equilibrium, then the calculated zircon saturation temperature (ZST; Watson and Harrison, 1983) and the temperature to which the inclusion was heated should be in agreement. The reasonably good agreement between TH and ZST (Table 1), suggests that the zircon and coexisting melt were in equilibrium at TH.

Observed differences between ZST and TH are most likely the result of analytical errors associated with determination of Zr concentrations by EPMA. To test this hypothesis, the concentration of Zr necessary to bring the calculated ZST into

Fig. 2. Electron microprobe traverse showing Al_2O_3 concentration (wt.%) in melt inclusion #1 to 1 and host zircon. Shaded portions denote analyses that include both zircon and the melt inclusion (MI). The beam diameter during analysis was approximately 2 μm.
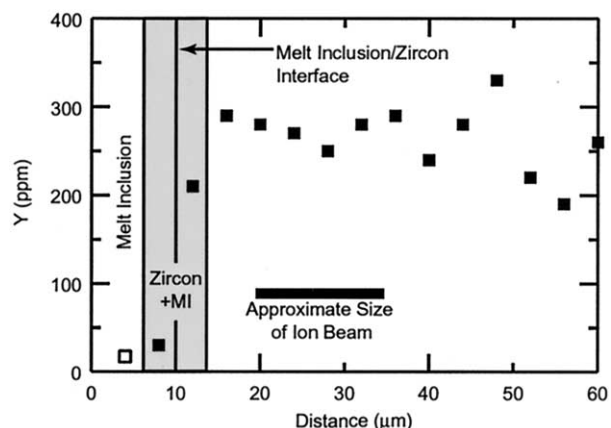

Fig. 3. Electron microprobe traverse showing Y concentration (ppm) in zircon adjacent to melt inclusion #8 shown in Fig. 1. Also shown is the size of the ion beam used during SIMS analysis. The zircon appears to be relatively homogeneous in Y at the scale of the ion beam.

agreement with the measured TH was determined and compared to the measured Zr concentration. The median difference is 35%, not including inclusion #B2 that was heated in one single step, and inclusion #8 which requires a 300% error in measured Zr (Table 1). We interpret these results to indicate that the compositions of the melt inclusions represent the composition of a melt that is in equilibrium with zircon at TH. Finally, we note that the measured TH is not necessarily the trapping temperature. However, whether TH does or does not approximate the trapping temperature is immaterial given the goals of this study. All that matters is that the melt in the inclusion is in equilibrium with the zircon crucible in which it is contained.

Petrographic observation, back-scattered electron images (Fig. 1), electron microprobe major element traverses (Fig. 2) and electron microprobe trace element traverses (Fig. 3) confirm the chemical homogeneity of individual inclusions and the host zircons. Additionally, three of the melt inclusions were large enough for duplicate SIMS analyses and show reasonably good reproducibility (Fig. 4). On the basis of major element compositions, all homogenized melt inclusions from this study are calc-alkaline and chemically classified as granite (Barker, 1979), with SiO_2 ranging between 75.88 and 79.40 wt.% (Fig. 5; Table 1) calculated on an anhydrous basis. The Na_2O and K_2O contents of the melt inclusions show little correlation with SiO_2 content (Fig. 5). Most of the melt inclusions are peraluminous with the exception of inclusions #1 to 11 and #16, which have aluminum saturation indices of 0.86 and 0.95, respectively.

Chondrite-normalized (Nakamura, 1974) REE abundances in melt inclusions and immediately adjacent zircon host are shown in Figures 6a and b, respectively. The melt inclusions display smooth U-shaped chondrite-normalized REE patterns (Fig. 6a) that differ significantly from the host zircons. Moreover, zircon is enriched in HREE (Dy, Er, Yb), but depleted in the LREE La, relative to melt (Fig. 6b). While REE abundances show significant variation from one zircon to the next, the patterns are similar to one another and are simply displaced to higher or lower values. With the exception of Ce, concentrations of REE in zircons increase smoothly from La to Yb. The zircons display large positive Ce anomalies ($Ce/Ce* = Ce_N/\sqrt{[La_N \times Nd_N]}$) ranging from 3.16 to 15.8 (average = 9.4) and La_N/Yb_N ranging from 0.00093 to 0.00927 (Table 2). Total REE of the zircons (for the seven REE analyzed in this study) ranges from 263 to 2411 ppm (average = 910 ppm). This range is consistent with abundances for these same REE measured in zircons from other granitic rocks (Hoskin et al., 2000).

Melt inclusion La_N/Yb_N ratios range from 0.63 to 7.51 (average = 2.61; Table 1) indicating that LREE are not strongly fractionated from HREE, as evidenced by the chondrite-normalized REE patterns on Fig. 6a. The highest La_N/Yb_N ratios correspond to inclusions with the lowest Yb abundances. While the LREE are not strongly fractionated from the HREE in melt inclusions, LREE are somewhat fractionated from the middle REE (Fig. 6a) as indicated by La_N/Sm_N ratios that range from 4.3 to 9.8, with one value at 28.9 (average = 8.7).
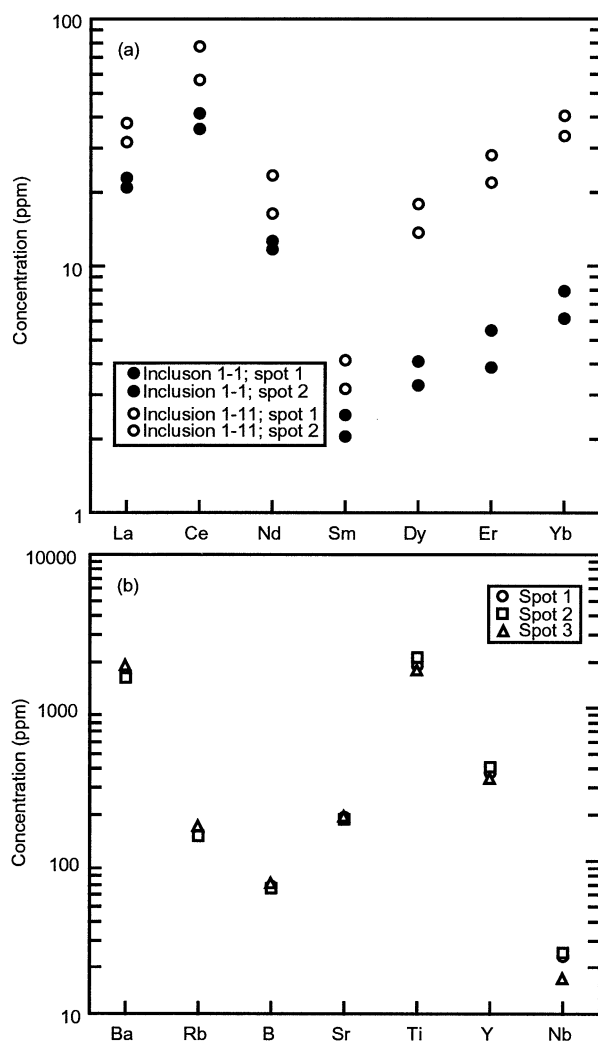

Fig. 4. Results of duplicate analyses of larger melt inclusions for (a) REE and (b) other trace elements documenting the homogeneity of individual melt inclusions.

5. ASSUMPTIONS INVOLVED WITH THE MIM TECHNIQUE

The determination of REE zircon/melt partition coefficients with the MIM technique involves several assumptions. First, it is assumed that the REE concentration of the trapped melt is not affected by boundary layer processes. Secondly, it is assumed that once the melt is trapped the inclusion represents a closed system and that the REE budget of the melt inclusion does not change, either through crystallization onto the walls of the inclusion or through diffusive loss (or gain) of components (or that these changes can be accounted for or reversed in the laboratory). Thirdly, it is assumed that the analytical techniques (homogenization of the crystallized melt inclusions, and electron and ion beam analyses) do not introduce errors. Below we test each of these assumptions to assess the validity of the MIM technique.

When a crystal grows from a melt, the concentration of compatible elements is depleted at the crystal/melt interface as these elements are incorporated into the growing crystal. Sim-
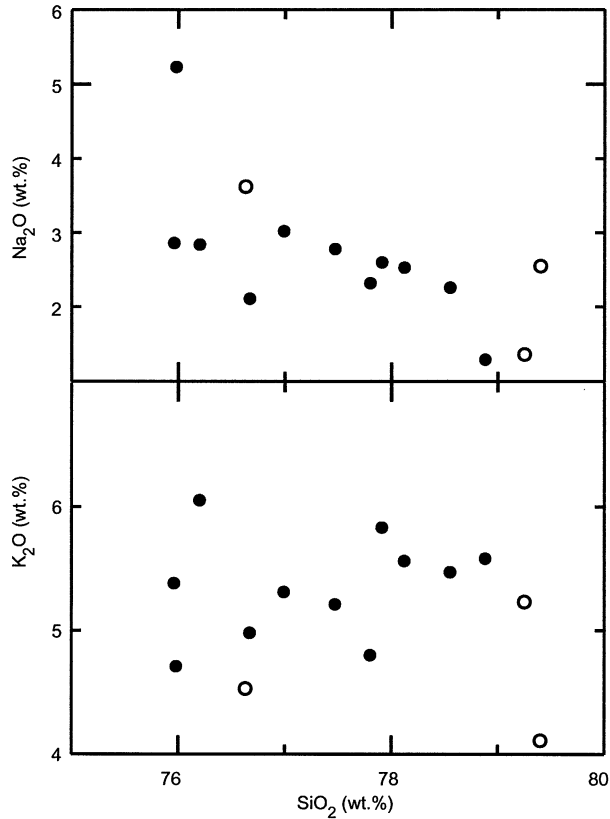
Fig. 5. Na_2O and K_2O concentration versus SiO_2 (wt.%) for melt inclusions reported in Table 1. The filled symbols represent inclusions analyzed for REE and the open symbols represent samples analyzed for other trace elements.
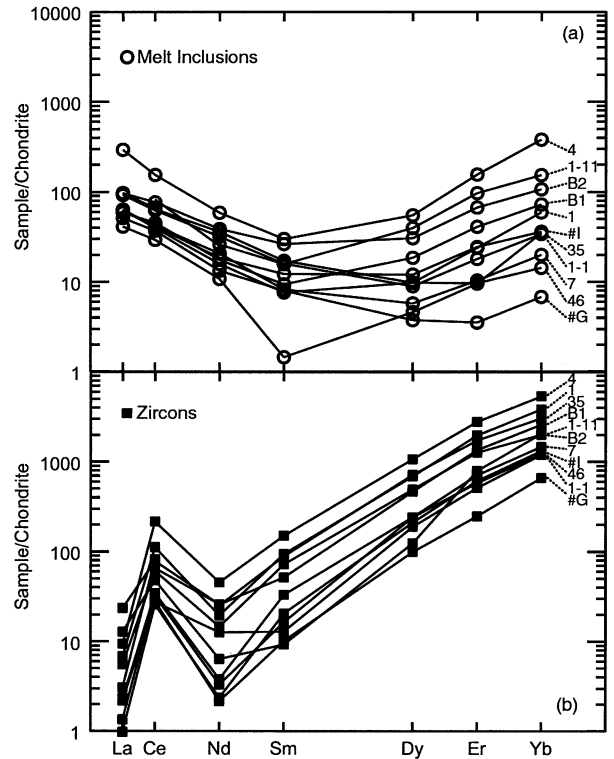

Fig. 6. Chondrite-normalized concentrations of REE in melt inclusions (a) and host zircons (b). Lines connect data from the same inclusion or zircon. The sample numbers for both melt inclusions and zircon are shown on the right. Data are listed in Tables 1 and 2.

ilarly, the incompatible elements accumulate in this narrow zone as they are excluded from the growing crystal. The rate at which compatible elements can be replaced in this boundary layer, and the rate at which incompatible elements can be removed, depends upon the diffusion rates for these elements in the melt phase and crystal growth rates (Watson et al., 1982; Bacon, 1989). Based on studies of melt inclusions, the effect of chemical gradients within the boundary layer on melt inclusion compositions is thought to be small for most inclusions greater than ≈25 μm (Anderson, 1974; Lowenstern, 1995) and can be ignored for inclusions >50 μm in diameter (Lu et al., 1995). Webster and Rebbert (2001) found no boundary layer effects in melt inclusions smaller than 70 μm in maximum dimension in quartz from Ascension Island.

In the present study, most of the inclusions analyzed were between 25 to 50 μm. While it is not possible to prove that these inclusions were not affected by boundary layer processes during trapping, systematic variations in REE concentrations with size over the limited range of sizes examined were not observed. Further evidence that boundary layer processes have not significantly affected the trace element chemistry of the inclusions is that the least compatible REE (La) does not appear to be enriched (relative to typical granitic compositions) in the melt inclusions, and the most compatible REE (Yb) does not appear to be depleted (Fig. 6a), as would be expected if boundary layer processes were operating. Thus, we conclude that the composition of the melt trapped in the inclusions was not significantly affected by boundary layer processes.

The second assumption involved in the use of melt inclusions to determine mineral/melt partitioning behavior is that the melt inclusions remain closed systems after trapping. However, under some conditions, melt trapped in an inclusion may continue to equilibrate with the bulk melt surrounding the host mineral as a result of diffusive exchange of components. For example, it is well known that the water content (Sobolev et al., 1990; Lowenstern and Mahood, 1991; Lu, 1991; Vityk et al., 2000) and the major element content (Gaetani and Watson, 2000; Danyushevsky et al., 2000, 2002) of melt and fluid inclusions can change, either during slow cooling in nature or during prolonged heating experiments in the laboratory. Qin et al. (1992) determined that for a species with a partition coefficient, k, ≥1, contained in an inclusion of diameter a in a host mineral of diameter b, with a size ratio (a/b) of 0.01, the dimensionless time τ (=Dt/b^2; where D is the diffusion coefficient, t is time, and b is the host crystal diameter) required to reach 10% reequilibration is approximately 0.1. Thus, for a crystal 1 mm in diameter containing a melt inclusion 10 μm in diameter, and a diffusion coefficient of 10^{-29} m^2 sec^{-1} (diffusion coefficient for Lu in zircon at 800°C; Cherniak et al., 1997), approximately 10^{22} seconds, or 3×10^{14} years is required for the Lu concentration in the melt inclusion to reach 10% reequilibration with the external melt.

The amount of time required to reach a given degree of reequilibration increases as the diffusion coefficient decreases.

Table 3. Partition coefficients (D_{REE}) calculated from REE abundances of melt inclusions and coexisting zircon hosts. Data listed in Tables 1 and 2.

	D_{La}	D_{Ce}	D_{Nd}	D_{Sm}	D_{Dy}	D_{Er}	D_{Yb}
#1	0.05	2.06	1.58	11.61	72.98	72.39	51.52
#1-1	0.04	0.83	0.2	2.7	20.09	29	40.63
#B1	0.07	1.46	0.5	3.56	22.45	29.35	35.88
#B2	0.22	0.99	0.53	4.14	16.79	21.09	21.9
#4	0.03	1.4	0.77	5.02	19.41	17.89	14.04
#7	0.02	0.61	0.11	2.49	36.56	58.88	66.1
#1-11	0.06	0.93	0.56	4.58	12.37	13.07	13.04
#35	0.26	1.26	0.81	3.24	51.95	74.99	76.32
#46	0.02	0.43	0.35	0.75	19.31	52.72	82.29
#I	0.03	1.1	0.31	11.24	52.31	60.74	35.11
#G	0.05	0.75	0.16	1.27	26.42	70	96.72
Median	0.05	0.99	0.5	3.56	22.45	52.72	40.63

According to Cherniak et al. (1997), the diffusion coefficients decrease with decreasing atomic number for the REE; thus, the time required for all other REE lighter than Lu will be longer than that calculated above for Lu. Moreover, as trace element compatibility increases, the time to reach a given degree of reequilibration decreases. Using the data of Qin et al. (1992), the time required to reach a given degree of reequilibration for the inclusions in this study will be *greater* than that calculated for the 10 μm inclusion above, or *greater* than ~300 trillion years! In summary, the theoretical model of Qin et al. (1992) indicates that the possible change in the REE concentration of melt inclusions in zircon as a result of diffusion is essentially nil, even if the melt inclusions had been maintained at the formation temperature from their time of formation until the present.

As discussed above, compositions of melt inclusions in this study were unlikely to have been affected by boundary layer processes or diffusion-related reequilibration of the melts following entrapment as inclusions. This allows us to focus on errors resulting from homogenizing the inclusions, and analytical errors. All of the melt inclusions in this study crystallized as a result of the slow cooling following entrapment in the plutonic environment. During the course of heating the inclusions to produce a homogeneous glass for microbeam analysis, it was assumed that any zircon that precipitated on the walls following entrapment would have been incorporated back into the melt during the homogenization process. Furthermore, the amount of zircon precipitated during cooling (or dissolved during later reheating) is controlled by zircon solubility in the melt as a function of temperature (and melt composition). The relatively good agreement between measured THs and temperatures predicted from the zircon saturation equation of Watson and Harrison (1983) (using our measured Zr concentrations in the melt inclusions; Table 1), suggests that the melt inclusions equilibrated with the zircon host during the homogenization process.

Potential errors associated with dissolving too much or too little zircon host during homogenization may be estimated by considering the effect on the ZST (Watson and Harrison, 1983). For example, application of the zircon saturation equation to melt inclusion #G, which contains 649 ppm Zr (Table 1), yields a temperature (937°C) that is in excellent agreement with the measured homogenization temperature (950°C). If it is assumed that during cooling and crystallization of the melt that all of the Zr in the original melt was incorporated into zircon

crystallizing on the walls, and if only 10% (65 ppm) of the Zr that precipitated was re-incorporated into the melt during homogenization, then the calculated ZST would be 721°C. Similarly, overheating the inclusion and adding 1% excess zircon (containing ~500000 ppm Zr) to melt inclusion #G (Table 1) would change the Zr concentration in the melt from 649 to 5573 ppm. The ZST predicted from this Zr concentration is 1242°C. Note that dissolving excess zircon during homogenization is analogous to placing the ion beam partially on the melt inclusion and partially on the host zircon during SIMS analysis. Incorporation of excess zircon in the inclusion, either from overheating or incorrect beam placement, would result in ZST significantly different from those calculated for the melt inclusions (and significantly different from the measured homogenization temperatures), and is not supported by the measured Zr concentrations of the melt inclusions (Table 1).

6. TRACE ELEMENT PARTITIONING

6.1. Rare Earth Elements

Zircon/melt partition coefficients for each inclusion/host pair were calculated from SIMS data and are listed in Table 3 and shown on Figure 7a. Zircon/melt partition coefficients determined in this study increase with increasing atomic number—the trend is similar to that determined by other workers (Nagasawa, 1970; Hinton and Upton, 1991; Watson, 1980; Fujimaki, 1986; Guo et al., 1996; Hoskin et al., 2000; and others; see also the compilation at the GERM website at: http://earthref.org/GERM/). While the concentrations of individual trace elements vary by more than one order of magnitude from one melt inclusion to the next (Fig. 6a; Table 1), and from one zircon crystal to the next (Fig. 6b; Table 2), the calculated partition coefficients for individual REE generally vary by less than one order of magnitude (Table 3), reflecting the fact that melt inclusions with the highest REE abundances are generally associated with zircons with the highest REE abundances. For example, the La concentration in melt inclusions varies from ~14 to 97 ppm (Table 1), and the La concentration in host zircon ranges from 0.4 to 7.89 ppm. Assuming that the La concentrations in melt inclusions and zircon host vary randomly, one would expect a range in calculated D_{La} of greater than two orders of magnitude (from 0.0041 to 0.563). However, partition coefficients calculated for the two end-member melt concentrations reported above are identical at
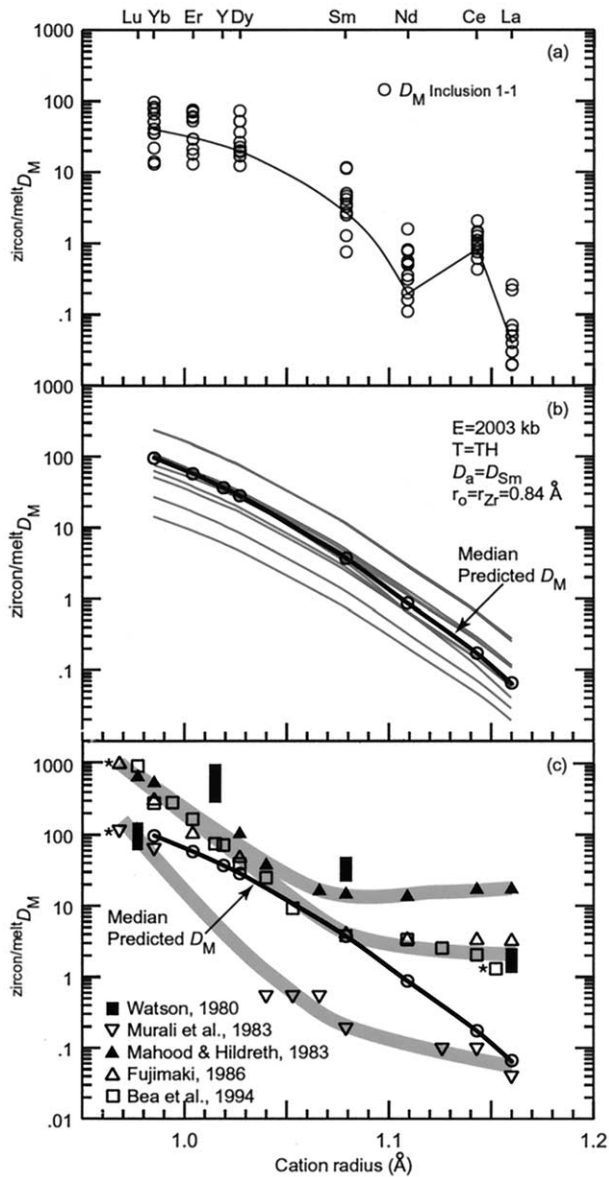
Fig. 7. (a) Zircon/melt partition coefficients (D_{REE}) calculated from data listed in Tables 1 and 2. The calculated values are also listed in Table 3. The line connects values for melt inclusion #1 to 1, showing the expected parabolic trend (see Fig. 7b) as well as the significant Ce anomaly. Similar trends are exhibited by the other ten inclusions, but are not shown because the overlap in data makes it difficult to identify lines connecting individual inclusions.(b) D_{REE} predicted by the Brice, 1975 equation for rare earth elements and Y calculated from melt inclusion/zircon pairs of this study at a temperature corresponding to the homogenization temperature listed in Table 1. The heavy solid line shows the median predicted D_M. (c) Comparison of median predicted D_M vs. cation radius from this study with previously published results. The upper shaded line shows the trend for the data of Mahood and Hildreth (1983), the middle shaded line approximates the trends for the data of Fujimaki (1986) and Bea et al. (1994), and the lower shaded line shows the trend for the data of Murali et al. (1983). Three of the data points (denoted by asterisks) have been offset to the left along the cation radius axis to avoid overlapping of the symbols. Cation radii are from Shannon (1976).

0.03 (Table 4), and the total range in D_{La} is only about one order of magnitude (from 0.02 to 0.26; Table 3). The variations in partition coefficients determined here are consistent with those determined in both experimental studies (Watson, 1980) and from analyses of natural samples Mahood and Hildreth (1983). Thus, Watson (1980) reports a range in D_{Lu} from less than 20 to greater than 100 based on experimental results, and Mahood and Hildreth (1983) report a range in D_{La} from 7.2 to 26.6 based on analyses of zircon and rhyolitic glass from the Bishop Tuff.

The range in REE contents of melt inclusions and zircon shown in Figures 6a and 6b, respectively, reflect the natural variation in REE in the QIC igneous system with time. As noted above, zircon is believed to have formed over a significant portion of the crystallization history of the QIC. As such, the REE budgets of the melt and the zircons precipitating from that melt would be expected to vary with time as the melts are depleted in REE by zircon and other crystallizing phases. The variation observed at the individual melt inclusion/single zircon host scale in this study is analogous to the variation observed at the bulk rock (or glass)/zircon separate scale in some other studies (cf., Mahood and Hildreth, 1983).

The zircon lattice contains two sites for cation substitution, a tetragonal Si site and a larger triangular dodecahedral Zr^{4+} site (Speer, 1982). HREE enrichment is due to substitution into the site containing Zr^{4+} (0.84 Å) (Speer, 1982; ionic radii in VIII coordination are from Shannon, 1976). Xenotime-type substitution (whereby an REE^{3+} ion and a P^{5+} ion substitute for Zr^{4+} and Si^{4+}) has been reported in zircon (e.g., Speer, 1982; Hoskin et al., 2000; Hanchar et al., 2001; Finch et al., 2001). The P content of the zircons from this study is below detection limits (Table 2).

The compatibility of REE^{3+} in zircon is controlled mostly by REE^{3+} radii and to a lesser extent the charge of the ion (Hinton and Upton, 1991; Guo et al., 1996). As such, D_{REE} increase from La through Yb as the ionic radii decrease from 1.16 Å to 0.985 Å, and approach the ionic radius of Zr^{4+} (0.84 Å). However, due to differences in the ionic radius of Zr^{4+} compared to the REE^{3+}, substitution of REE^{3+} for Zr^{4+} in the zircon lattice results in lattice strain compensated by the excess free energy required to replace Zr^{4+} with substantially larger REE^{3+} (Blundy and Wood, 1994).

Blundy and Wood (1994) and Wood and Blundy (1997) describe a method based on equations developed by Brice (1975) to predict the partitioning behavior in mineral/melt systems. The predicted partition coefficients should display a parabolic form when log $^{mineral/melt}D_M$ is plotted versus ionic radii for a group of isovalent cations. The maximum on the parabola defines the optimum cation size that fits into the site involved in the partitioning (Onuma et al., 1968), and is generally close to the size of the major cation that is being replaced. For zircon, the maximum on the parabola should be at approximately 0.84 Å, which corresponds to the ionic radius of Zr^{4+} in the zircon structure (Speer, 1982; Shannon, 1976).

The D_{REE} values predicted from the Brice (1975) equation are compared to D_{REE} values calculated from melt inclusion and zircon analyses on Figure 7. The predicted D_{REE} were obtained using 0.84 Å as the optimum cation radius (r_o) of the Zr site onto which partitioning occurs, a Young's modulus for the Zr site (E) of 2003 kb, and temperature = TH. The Young's

Table 4. D_{REE} calculated for lowest (top) and highest (bottom) La, Sm and Yb abundances in the melt inclusions. Data for the coexisting zircon are also shown.

[a]La_{MI}	[b]La_{zircon}	D_{La}	[a]Sm_{MI}	[b]Sm_{zircon}	D_{Sm}	[a]Yb_{MI}	[b]Yb_{zircon}	D_{Yb}
13.6	0.41	0.03	0.29	3.26	11.24	1.495	144.6	96.72
96.6	2.9	0.03	6.06	30.4	5.02	83.35	1170	14.04

[a] REE abundance in melt inclusion.
[b] REE abundance in zircon.

modulus was derived by fitting our partitioning data to Eqn. 10 of Wood and Blundy (1997), and then using the relationship between Young's modulus and bulk modulus described by Hazen and Finger (1979) and shown in Blundy and Wood (1994; their Fig. 3). The Brice (1975) model requires that the partition coefficient for one cation of the isovalent group be known to calculate partition coefficients for other elements of the isovalent group. In the model calculations here the value for D_{Sm} from each inclusion was used to represent the "known" (D_a) value for that inclusion (Table 3). The predicted values shown on Fig. 7b define only one limb of the parabola because the Zr site (0.84 Å) is smaller than the size of the smallest REE (Yb) measured; i.e., the maximum on the parabola is at a radius of 0.84 Å and lies off of the diagram to the left. The value predicted by the Brice (1975) equation lies within the range of measured D_{REE} for all of the REE measured in this study, and the predicted values vary by less than one order of magnitude from the median D_{REE} values reported in Table 3 (except for Ce, which is discussed in more detail below).

Partition coefficients predicted by the Brice equation from the melt inclusion data are compared to published values on Figure 7c. As expected, all previous studies show an increase in compatibility with decreasing ionic radius. However, in contrast to most previously published results (with the exception of the data of Murali et al., 1983), our data indicate that La and Nd behave incompatibly in felsic melts (i.e., $D_M < 1$). Petrogenetic implications of this difference are considered later. Most previous studies show flat partitioning patterns for the light through middle REE (i.e., no change in the partition coefficient with ionic radius), whereas our results indicate continuously decreasing compatibility from Yb through La as predicted by the Brice equation. Watson (1980) shows the same general pattern as in the present study (Fig. 7c), although the absolute values for D_M differ by more than one order of magnitude for La (and less for the other REE) between the two studies. These differences are currently unresolved but are possibly related to the differing melt compositions in these two studies. Note that the D_{LREE} trends from previously published studies are the opposite of that predicted by the Brice (1975) model. Related to this, Hinton and Upton (1991) noted that many published D_{LREE} are higher than would be expected if REE substitution is a function exclusively of ionic radius and attributed this difference to impurities contained in mineral separates in those studies.

Differences described above reflect the different experimental and analytical techniques employed in these various studies. Hinton and Upton (1991), Maas et al. (1992) and Guo et al. (1996) suggested that many of the reported D_M values are incorrect owing to bulk analysis of zircons containing solid inclusions or areas of alteration, and other workers have documented the significant effects of small amounts of contaminants during analysis (Michael, 1988; Beattie, 1994). Our calculations indicate that including less than 1% of an accessory mineral that strongly partitions the LREE (e.g., allanite or monazite) within the bulk sample could produce the observed flat D_{LREE} pattern reported by other workers (Fig. 7c). We suggest that the good agreement between our measured values and model results predicted by the Brice equation indicate that D_{REE} obtained using the MIM technique may be more reliable than those obtained from bulk analyses of mineral separates.

It is important to emphasize that partition coefficients in natural systems vary as a function of many parameters, including ionic potential, temperature, pressure, oxygen fugacity, crystal chemistry, and melt composition, including water content (Onuma et al., 1968; Drake and Weill, 1975; Watson, 1977; Matsui et al., 1977; Philpotts, 1978; Hart and Davis, 1978; Lindstrom and Weill, 1978; Ryerson and Hess, 1978; Green and Pearson, 1983, 1986; Dunn, 1987; Blundy and Wood, 1991; Hill et al., 2000). A significant difference between melt inclusions studied here and melts (volcanic glass) studied by most other workers is the water content. As noted previously, melt inclusions studied here may contain up to 8 or 9 wt.% water, compared to concentrations generally less than 2 or 3 wt.% water in volcanic glass. Blundy (private communication, 2002) notes that water has the effect of lowering $^{cpx/melt}D_{REE}$ but that water has no effect on $^{garnet/melt}D_{REE}$. Blundy (private communication, 2002) further notes that zircon may behave more like garnet. Finally, it should be noted that Watson and Harrison (1983) saw no effect of water content on zircon solubility.

6.2. Other Trace Elements

Fewer analyses were conducted for the trace elements Ba, Rb, B, Sr, Ti, Y and Nb (Tables 1 and 2). Zircon/melt partition coefficients for these elements were calculated as described above for the REE, and are plotted on Figure 8 in terms of increasing compatibility. D_M values are listed in Table 5. As expected based on charge/size ratios, Ba, Rb, B and Sr behave incompatibly, whereas Y and Nb are highly compatible, with Ti showing moderate compatibility. These values are consistent with elevated Nb and Y concentrations often reported for zircon (cf., Hoskin et al., 2000), and with the single value for D_Y from Bea et al. (1994).

6.3. Positive Ce Anomalies in Zircon

Zircon commonly shows a positive Ce anomaly (e.g., Hinton and Upton, 1991), which has been interpreted to indicate the incorporation of Ce into zircon as Ce^{4+}. Because Ce^{4+} has the
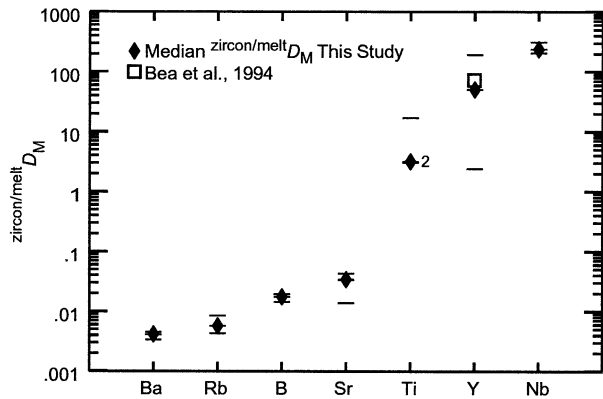
Fig. 8. D_M for trace elements calculated from zircon/melt inclusion pairs. The elements are plotted in terms of increasing compatibility in zircon. Tic marks indicate individual values, and the "2" adjacent to the tic mark for Ti indicates two data points with overlapping values. Also shown is a single value for D_Y from the literature (Bea et al., 1994).

same charge as the Zr^{4+} it replaces, and a similar ionic radius ($Ce^{4+} = 0.97$; $Zr^{4+} = 0.84$ Å), it is incorporated into the zircon structure much more readily than the larger Ce^{3+} ($Ce^{3+} = 1.143$ Å). Thus, the calculated partition coefficient for Ce (Fig. 7a) represents an apparent partition coefficient that includes both Ce^{3+} and Ce^{4+} (Hinton and Upton, 1991). The strong positive Ce anomalies in zircon (e.g., Murali et al., 1983; Hinton and Upton, 1991; Maas et al., 1992; Guo et al., 1996; Hoskin et al., 2000) indicate that Ce occurs in melts as both Ce^{4+} and Ce^{3+}, although Ce^{3+} dominates in terrestrial melts (Schreibber et al., 1980). Ce anomalies are absent in lunar zircons (Hinton and Myer, 1991) that formed under reducing conditions.

The expected partition coefficient assuming 100% Ce^{3+} was calculated using the Brice (1975) equation described earlier. Using the same values for the input parameters as described above for the other REE^{3+} gives $D_{Ce3+} = 0.14$ (Fig. 7b). The median value for the apparent partition coefficient for Ce determined from the MIM technique is 0.99 (Table 3). The partition coefficient for Ce^{4+} in zircon was predicted using the ionic radius for Ce^{4+} (0.97 Å), a Young's modulus (E) for the site of 4226 kb (based on the relationship between cation charge/site volume ratio (Z/d^3) and bulk modulus, after Hazen and Finger, 1979) and using $D_{Zr4+} = 1700$ (based on the average Zr concentration in the melt inclusions (Table 1) and host zircon (Table 2). Using these values, the Brice (1975) equation predicts $D_{Ce4+} = 102.6$.

The Ce^{4+}/Ce^{3+} ratio in the melt inclusions was estimated using the calculated D_{Ce4+} and D_{Ce3+} values, the apparent D_{Ce} values from Table 3, and Eqn. 2 from Hinton and Upton (1991).

The calculated Ce^{4+}/Ce^{3+} ratios range from 0.0029 to 0.0188, and (except for one value) show a systematic increase in Ce concentration in zircon with increasing Ce^{4+}/Ce^{3+} ratio in the melt. This is interpreted to indicate that zircons with the highest Ce content in the QIC crystallized from melts with the highest Ce^{4+}/Ce^{3+} ratios. The wide range in Ce concentration in zircon is likely the result of both variable total Ce and evolving Ce^{4+}/Ce^{3+} ratio in the melt during crystallization. It should be noted, however, that zircons with positive Ce anomalies (reflecting an elevated concentration of Ce^{4+} in the zircon) can be produced from melts with relatively low Ce^{4+}/Ce^{3+} ratios if other phases which preferentially remove Ce^{3+} from the melt are crystallizing at the same time as zircon (Hinton and Upton, 1991).

7. PETROGENETIC IMPLICATIONS

One important application of partition coefficients is for quantitative modeling of petrogenetic processes. In such calculations, relatively small errors in partition coefficients can have relatively large effects on model predictions. To illustrate this, we have modeled batch partial melting and fractional crystallization using the D_{La} and D_{Yb} determined in this study and compared these results to those predicted using the partition coefficients of Fujimaki (1986). We selected La and Yb for these calculations because published partition coefficients for these elements show the largest departure from results of the present study. We compared our results to those of Fujimaki (1986) because those values are widely used in published petrogenetic models.

The evolution of La and Yb during batch partial melting (Eqn. 11 of Shaw, 1970) of a mafic (amphibolite) protolith containing 16.1 ppm La and 4.2 ppm Yb is shown in Figure 9a. The La and Yb concentrations are taken from Thomas and Sinha (1999; their Table 5), and were obtained from analysis of an amphibolite thought to represent the source for the melts that formed the QIC. The model assumes a residual assemblage containing 75% clinopyroxene, 24.5% plagioclase and 0.5% zircon. For comparison, batch partial melting of a zircon-free residual assemblage containing 75% clinopyroxene, 25% plagioclase was modeled (Fig. 9a). The residual assemblages were selected in accordance with observed experimental partial melting residues (e.g., Beard and Lofgren, 1991; Rushmer, 1991; Wolf and Wyllie, 1994; Patiño-Douce and Beard, 1995), and use partition coefficients for clinopyroxene and plagioclase from Klein et al. (2000), Schnetzler and Philpotts (1970) and Fujimaki et al. (1984).

The melt generated by 10% partial melting of the zircon-free assemblage contains 6.1 ppm Yb and 83 ppm La (Fig. 9a). For the zircon-bearing assemblage, the melt generated by 10% partial melting contains 4.8 ppm Yb using the partition coef-

Table 5. D_M calculated from the 3 melt inclusions in Table 1 and REE abundances of coexisting zircon hosts.

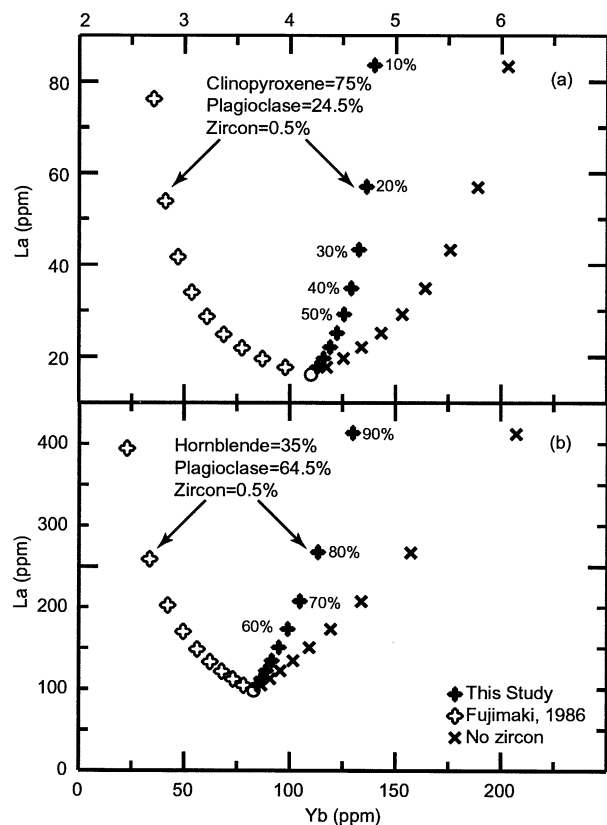|	D_{Ba}	D_{Rb}	D_B	D_{Sr}	D_{Ti}	D_Y	D_{Nb}
#8	0.003	0.008	0.019	0.034	3.30	50.2	312
#9	0.005	0.006	0.014	0.043	16.8	191	236
#16	0.004	0.004	0.017	0.014	3.15	2.39	204
Median	0.004	0.006	0.017	0.034	3.15	50.2	236

Fig. 9. Petrogenetic models for (a) batch partial melting (Shaw, 1970) and (b) fractional crystallization showing the effect of variation in D_{La} and D_{Yb} on melt evolution, using values from this study and from Fujimaki (1986). Also shown for comparison are model results without zircon in the residual assemblage for batch partial melting (a) and in the fractionation assemblage for fractional crystallization (b). The numbers next to the model values indicate the mass percent melt generated for partial melting and the mass percent crystallization for fractional crystallization.

ficient from this study, but only 2.7 ppm Yb using the partition coefficient of Fujimaki (1986). The La concentrations are not significantly different between the zircon-free or zircon-bearing models, or using the Fujimaki data or our data. As shown on Fig. 9a, Yb is most incompatible in the residue for the model with 0% zircon in the residual assemblage, as well as in the model including 0.5% zircon and using the D_{REE} from this study. However, using D_{REE} of Fujimaki (1986) results in Yb depletion in the melt for the zircon-bearing case.

Fractional crystallization (Greenland, 1970) was modeled using melt inclusion #4 (Table 1) as the parental melt, and published partition coefficients for hornblende and plagioclase (Fujimaki et al., 1984; Green and Pearson, 1985). Melt inclusion #4 was selected because it has relatively high REE concentrations compared to the other melt inclusions studied. As shown on Figure 9b, Yb is conserved in the melt for the model with 0% zircon in the fractionated assemblage, as well as in the model including 0.5% zircon and using the D_{REE} from this study. However, using D_{REE} of Fujimaki (1986) results in a strongly Yb-depleted melt for the zircon-bearing case. These calculations illustrate the significant differences that might result using different values for REE partition coefficients in

petrogenetic models and highlight the need for accurate partitioning data for use in these models.

8. LIMITATIONS OF THE MELT INCLUSION-MINERAL (MIM) TECHNIQUE

The MIM technique described above to determine trace element partition coefficients is valid for the mineral zircon. The validity of the technique is based on the fact that diffusion rates for REE in zircon are extremely slow (Cherniak et al., 1997). Thus, the REE concentrations of melt inclusions and host zircon are unlikely to change as a result of diffusion following trapping. However, similar behavior is not expected for all minerals from all environments. While Sobolev et al. (1996) were able to determine trace element partitioning behavior between basaltic melt and clinopyroxene based on melt inclusions in clinopyroxene from the Upper lavas of the Troodos Massif, Cyprus, it is not clear that the approach would have worked for clinopyroxene (or other minerals) that cooled more slowly in a deep-seated environment. We also note that the diffusion coefficients for other trace elements (Ba, Rb, B, Sr, Ti Y and Nb) examined in this study are not as well constrained as those for REE in zircon, and could have been modified by later processes. Finally, we note that zircon immediately surrounding the melt inclusions in this study appears to be relatively homogeneous in trace element concentration over a distance of at least several tens of microns (Fig. 3). However, many zircons described in the literature are zoned on a fine scale (e.g., Heaman et al., 1990). If zircon exhibits zoning on a scale that is smaller than the size of the ion beam (approximately 10 to 20 μm), use of the technique described here might not provide reliable partitioning information.

Cherniak et al. (1997) note that the closure temperature for REE diffusion in zircon is higher than that for other minerals (such as diopside, titanite, garnet and apatite), suggesting that these other minerals would continue to exchange REE with the surrounding bulk melt to a lower temperature compared to zircon (Qin et al., 1992). Based on low ionic porosity, Dahl (1997; see also Lee et al., 1997) estimates closure temperatures for Pb in zircon that are higher than those for Pb in Ca-clinopyroxene, epidote, monazite and xenotime, but lower than for staurolite and garnet. The MIM technique should only be used to determine partitioning behavior of minerals with low ionic diffusivities, low ionic porosity and high closure temperatures, and/or from environments in which postentrapment cooling was rapid.

9. CONCLUSIONS

Melt inclusions in zircon have been used to determine the partitioning behavior of REE in the zircon/granitic melt system. Due to the refractory nature of zircon and the slow diffusivities of trace elements through the crystal lattice, REE abundances measured in zircons today represent those present during crystal growth from the melt. Trace element partitioning is unaffected by postentrapment modifications and laboratory procedures. Partition coefficients for HREE determined using the MIM technique are in general agreement with published values, whereas, partition coefficients for LREE obtained in this study are significantly lower than most published values. D_{REE} determined from the MIM technique are consistent with the Brice

model that relates the partition coefficient to the size and elasticity of crystallographic sites. Positive Ce anomalies in zircons are related to the presence of both Ce^{3+} and Ce^{4+} in the melts from which the zircons crystallized. The Ce^{4+}/Ce^{3+} ratio of the melt has been predicted from the measured apparent partition coefficient and partition coefficients for Ce^{3+} and Ce^{4+} calculated using the Brice equation.

During fractional crystallization, removal of an assemblage containing 35% hornblende, 64.5% plagioclase and 0.5% zircon yields a bulk distribution coefficient of 1.6 for Yb, using D_{REE} reported by Fujimaki (1986). However, using the D_M values from this study predicts that Yb will be conserved in the melt (i.e., bulk distribution coefficient $<$ 1). The net result is that the predicted melt compositions will follow significantly different evolutionary paths during crystallization. We recognize that no single mineral controls the trace element evolution during separation of crystals from melt, and we are not proposing that zircon alone determines the REE budget of the system. Rather, the purpose of this study is to further document the application of the MIM technique to determine trace element partitioning behavior in mineral-melt systems. With the noted precautions taken, the MIM technique provides a robust and simple technique for determination of partitioning behavior in other mineral/melt systems.

Associate editor: F. J. Ryerson

REFERENCES

Anderson A. T. (1974) Evidence for a picritic, volatile-rich magma beneath Mt. Shasta, California. *J. Petrol.* **15,** 243–267.

Arth J. G. (1976) Behavior of trace elements during magmatic processes-a summary of theoretical models and their applications. *J. Res. U. S. Geol. Surv.* **4,** 41–47.

Bacon C. R. (1989) Crystallization of accessory phases in magmas by local saturation adjacent to phenocrysts. *Geochim. Cosmochim. Acta.* **53,** 1055–1066.

Barker F. (1979) Trondhjemites: definition, environment and hypothesis of origin. In *Trondhjemites, dacites and related rocks* (ed. F. Barker), pp. 1–12. Elsevier.

Bea F. (1996) Residence of REE, Y, Th and U in granites and crustal protoliths; implications for the chemistry of crustal melts. *J. Petrol.* **37,** 521–552.

Bea F., Pereira M. D., and Stroh A. (1994) Mineral/leucosome trace-element partitioning in a peraluminous migmatite (a laser ablation-ICP-MS study). *Chem. Geol.* **117,** 291–312.

Beard J. S. and Lofgren G. E. (1991) Dehydration-melting and water-saturated melting of basaltic and andesitic greenstones and amphibolites at 1, 3, and 6.9 kb. *J. Petrol.* **32,** 365–401.

Beattie P. (1994) Systematics and energetics of trace-element partitioning between olivine and silicate melts: Implications for the nature of mineral/melt partitioning. *Chem. Geol.* **117,** 57–71.

Blundy J. D. and Wood B. J. (1991) Crystal-chemical controls on the partitioning of Sr and Ba between plagioclase feldspars, silicate melts and hydrothermal solutions. *Geochim. Cosmochim. Acta.* **55,** 193–209.

Blundy J. and Wood B. (1994) Prediction of crystal-melt partition coefficients from elastic moduli. *Nature* **372,** 452–454.

CircularBrew D. A. and Ford A. B. (1981) The Coast plutonic sill, southeastern Alaska. *The U.S. Geologic Survey in Alaska-accomplishments during 1980,* vol. 823-B (eds. N. R. D. Albert and T. L. Hudson), pp. B99–B102. U.S. Geol. Surv..

Brice J. C. (1975) Some thermodynamic aspects of the growth of strained crystals. *J. Crystal Growth.* **28,** 249–253.

Brooks C. K., Henderson P., and Ronsbo J. G. (1981) Rare earth element partitioning between allanite and glass in the obsidian of Sandy Braes, northern Ireland. *Min. Mag.* **44,** 157–160.

Cherniak D. J., Hanchar J. M., and Watson E. B. (1997) Rare-earth diffusion in zircon. *Chem. Geol.* **134,** 289–301.

Chesner C. A. (1998) Petrogenesis of the Toba Tuffs, Sumatra, Indonesia. *J. Petrol.* **39,** 397–438.

Chesner C. A. and Ettlinger A. D. (1989) Composition of allanite from the Toba tuffs, Sumatra, Indonesia. *Am. Mineral.* **74,** 750–758.

Chupin S. V., Chupin V. P., Barton J. M., and Barton E. S. (1998) Archean melt inclusions in zircon from quartzite and granitic orthogneiss from South Africa: magma compositions and probable sources of protoliths. *Eur. J. Min.* **10,** 1241–1251.

Crawford M. L., Hollister L. S., and Woodsworth G. J. (1987) Crustal deformation and regional metamorphism across a terrane boundary, Coast Plutonic Complex, Br. *Columbia. Tectonics.* **6,** 343–361.

Dahl P. S. (1997) A crystal-chemical basis for Pb retention and fission-track annealing systematics in U-bearing minerals, with implications for geochronology. *Earth Planet. Sci. Lett.* **150,** 277–290.

Danyushevsky L. V., Della-Pasqua F. N., and Sokolov S. (2000) Re-equilibration of melt inclusions trapped by magnesian olivine phenocrysts from subduction-related magmas: petrological implications. *Contrib. Mineral. Petrol.* **138,** 68–83.

Danyushevsky L. V., McNeill A. W. and Sobolev A. V. (2002). Experimental and petrological studies of melt inclusions in phenocrysts from mantle-derived magmas: an overview of techniques, advantages and complications. *Chem. Geol.* **183,** 5–24.

Devine J. D., Gardener J. E., Brack H. P., Layne G. D., and Rutherford M. J. (1995) Comparison of microanalytical methods for estimating H_2O contents of silicic volcanic glasses. *Am. Mineral.* **80,** 319–328.

Drake M. J. and Weill D. F. (1975) Partition of Sr, Ba, Ca, Y, Eu $^{2+}$, Eu $^{3+}$, and other REE between plagioclase feldspar and magmatic liquid; an experimental study. *Geochim. Cosmochim. Acta.* **39,** 689–712.

Dunn T. (1987) Partitioning of Hf, Lu, Ti, and Mn between olivine, clinopyroxene and basaltic liquid. *Contrib. Mineral. Petrol.* **96,** 476–484.

Finch R. J., Hanchar J. M., Hoskin P. W. O., and Burns P. C. (2001) Rare earth elements in synthetic zircon: Part 2. A single-crystal X-ray study of xenotime substitution. *Am. Mineral.* **86,** 681–689.

Fujimaki H. (1986) Partition coefficients of Hf, Zr, and REE between zircon, apatite, and liquid. *Contrib. Mineral. Petrol.* **94,** 42–45.

Fujimaki H., Tatsumoto M., and Aoki K (1984) Partition coefficients of Hf, Zr and REE between phenocrysts and groundmass. *J. Geophys. Res.* **89,** (Suppl.) B662–B672.

Gaetani G. A. and Watson E. B. (2000) Open system behavior of olivine-hosted melt inclusions. *Earth Planet. Sci. Lett.* **183,** 27–41.

Gehrels G. E., McClelland W. C., Samson S. D., Patchett P. J., and Brew D. A. (1991) U-Pb geochronology and tectonic significance of late Cretaceous Early Tertiary plutons in the northern Coast Mountains batholith. *Can. J. Earth Sci.* **28,** 899–911.

Green T. H. and Pearson N. J. (1983) Effect of pressure on rare earth element partition coefficients in common magmas. *Nature* **305,** 414–416.

Green T. H. and Pearson N. J. (1985) Experimental determination of REE partition coefficients between amphibole and basaltic liquids at high pressure. *Geochim. Cosmochim. Acta* **49,** 1465–1468.

Green T. H. and Pearson N. J. (1986) Rare-earth element partitioning between sphene and coexisting silicate liquid at high pressure and temperature. *Chem. Geol.* **55,** 105–119.

Green T. H. and Pearson N. J. (1987) An experimental study of Nb and Ta partitioning between Ti-rich minerals and silicate liquid at high pressure and temperature. *Geochim. Cosmochim. Acta* **51,** 55–62.

Greenland L. P. (1970) An equation for trace element distribution during magmatic crystallization. *Am. Mineral.* **55,** 455–465.

Gromet L. P. and Silver L. T. (1983) Rare earth element distributions among minerals in a granodiorite and their petrogenetic implications. *Geochim. Cosmochim. Acta* **47,** 925–939.

Guo J., O'Reilly S. Y., and Griffin W. L. (1996) Zircon inclusions in corundum megacrysts: I. Trace element geochemistry and clues to the origin of corundum megacrysts in alkali basalts. *Geochim. Cosmochim. Acta* **60,** 2347–2363.

Hanchar J. M., Finch R. J., Hoskin P. W. O., Watson E. B., Cherniak D. J., and Mariano A. N. (2001) Rare earth elements in synthetic zircon: Part 1. Synthesis, and rare earth element and phosphorous doping. *Am. Mineral.* **86,** 667–680.

Hart S. R. and Davis K. E. (1978) Nickel partitioning between olivine and silicate melt. *Earth Planet. Sci. Lett.* **40,** 203–219.

Hazen R. M. and Finger L. W. (1979) Bulk modulus-volume relationship for cation-anion polyhedra. *J. Geophys. Res.* **84,** 6723–6728.

Heaman L. M., Bowins R., and Crocket J. (1990) The chemical composition of igneous zircon suites: Implications for geochemical tracer studies. *Geochim. Cosmochim. Acta* **54,** 1597–1607.

Hill E., Wood B. J., and Blundy J. D. (2000) The effect of Ca-Tschermaks component on trace element partitioning between clinopyroxene and silicate melt. *Lithos.* **53,** 203–215.

Hinton R. W. and Myer C (1991) Ion probe analysis of zircon and yttrobetafite in a lunar granite. *Lunar Planet. Sci.* **XXII,** 575–576.

Hinton R. W. and Upton B. G. J. (1991) The chemistry of zircon: Variations within and between large crystals from syenite and alkali basalt xenoliths. *Geochim. Cosmochim. Acta* **55,** 3287–3302.

Hoskin P. W. O., Kinny P. D., Wyborn D., and Chappell B. W. (2000) Identifying accessory mineral saturation during differentiation in granitoid magmas: an integrated approach. *J. Petrol.* **41,** 1365–1396.

Hutchison W. W. (1982) Geology of the Prince Rupert-Skeena map area, British Columbia. *Geol. Surv. Canada*, Memoir 394.

Irving A. J. and Frey F. A. (1984) Trace element abundances in megacrysts and their host basalts: Constraints on partition coefficients and megacryst genesis. *Geochim. Cosmochim. Acta* **48,** 1201–1221.

Klein M., Stosch H. -G., Seck H. A., and Shimizu N. (2000) Experimental partitioning of high field strength and rare earth elements between clinopyroxene and garnet in andesitic and tonalitic systems. *Geochim. Cosmochim. Acta* **64,** 99–115.

Klepeis K. A., Crawford M. L., and Gehrels G. (1998) Structural history of the crustal-scale Coast shear zone north of Portland Canal, Southeast Alaska and Br. *Columbia. J. Struct. Geol.* **20,** 883–904.

Lee J. K. W., Williams I. S., and Ellis D. J. (1997) Pb, U and Th diffusion in natural zircon. *Nature* **390,** 159–162.

Li Z. (1994) The silicate melt inclusions in igneous rocks. In *Fluid Inclusions in Minerals, Methods and Applications* (eds. B. De Vivo and M. L. Frezzotti), pp. 73–94.

Lindstrom D. J. and Weill D. F. (1978) Partitioning of transition metals between diopside and coexisting silicate liquids; I, Nickel, cobalt, and manganese. *Geochim. Cosmochim. Acta* **42,** 817–832.

Lowenstern J. B. (1994) Dissolved volatile concentrations in an ore-forming magma. *Geol.* **22,** 893–896.

Lowenstern J. B. (1995) Applications of silicate-melt inclusions to the study of magmatic volatiles. *Magma, Fluids, and Ore Deposits* (ed. F. H. Thompson), pp. 71–99. Mineral. Assoc. of Canada, Short Course Series 23.

Lowenstern J. B. and Mahood G. (1991) New data on magmatic H_2O contents of pantellerites, with implications for petrogenesis and eruptive dynamics at Pantelleria. *Bull. Volcanol.* **54,** 78–83.

Lu F. (1991) The Bishop Tuff: Origin of the high-silica rhyolite and its thermal and compositional zonations. Unpub. Ph. D. Dissertation, University of Chicago, Chicago, Illinois.

Lu F., Anderson A. T., and Davis A. M. (1992) New and larger sanidine/melt partition coefficients for Ba and Sr as determined by ion microprobe analyses of melt inclusions and their sanidine host crystals. *Geol. Soc. of America Abstracts with Programs* **24,** A44.

Lu F., Anderson A. T., and Davis A. M. (1995) Diffusional gradients at the crystal/melt interface and their effect on the compositions of melt inclusions. *J. Geol.* **103,** 591–597.

Maas R., Kinny P. D., Williams I. S., Froude D. O., and Compston W. (1992) The earth's oldest known crust: A geochronological and geochemical study of 3900 Ma detrital zircons from Mt. Narryer and Jack Hills, western Australia. *Geochim. Cosmochim. Acta.* **56,** 1281–1300.

Mahood G. and Hildreth W. (1983) Large partition coefficients for trace elements in high-silica rhyolites. *Geochim. Cosmochim. Acta.* **47,** 11–30.

Matsui Y., Onuma N., Nagasawa H., Higuchi H., and Banno S. (1977) Crystal structure control in trace element partition between crystal and magma. *Bulletin de la Societe Francaise de Mineralogie et de Cristallographie* **100,** 315–324.

Michael P. J. (1988) Partition coefficients for rare earth elements in mafic minerals of high silica rhyolites: The importance of accessory mineral inclusions. *Geochim. Cosmochim. Acta* **52,** 275–282.

Murali A. V., Parthasarathy R., Mahadevan T. M., and Sankar D. (1983) Trace element characteristics, REE patterns and partition coefficients of zircons from different geological environments-A case study on Indian zircons. *Geochim. Cosmochim. Acta* **47,** 2047–2052.

Nagasawa H. (1970) Rare earth concentrations in zircon and their host dacites and granites. *Earth Planet. Sci. Lett.* **9,** 359–364.

Nakamura N. (1974) Determination of REE, Ba, Fe, Mg, Na, and K in carbonaceous and ordinary chondrites. *Geochim. Cosmochim. Acta* **38,** 757–775.

O'Hara M. J., Fry N., and Prichard H. M. (2001) Minor phases as carriers of trace elements in non-modal crystal-liquid separation processes II: illustrations and bearing on behaviour of REE, U, Th and the PGE in igneous processes. *J. Petrol.* **42,** 1887–1910.

Onuma N., Higuchi H., Wakita H., and Nagasawa H. (1968) Trace element partitioning between two pyroxenes and the host lava. *Earth Planet. Sci. Lett.* **5,** 47–51.

Patiño-Douce A. E. and Beard J. S. (1995) Dehydration-melting of biotite gneiss and quartz amphibolite from 3 to 15 kb. *J. Petrol.* **36,** 707–738.

Pearce J. A. and Norry M. J. (1979) Petrogenetic implications of Ti, Zr, Y, and Nb variations in volcanic rocks. *Contrib. Mineral. Petrol.* **69,** 33–47.

Philpotts J. A. (1978) The law of constant rejection. *Geochim. Cosmochim. Acta* **42,** 909–920.

Qin Z., Fangqiong F., and Anderson T. (1992) Diffusive reequilibration of melt and fluid inclusions. *Am. Mineral.* **77,** 565–576.

Reed S. J. B. (1986) Ion microprobe determination of rare earth elements in accessory minerals. *Min. Mag.* **50,** 3–15.

Roedder E. (1984) *Fluid Inclusions* (ed. P. H. Ribbe), Mineralogical Society of America, Reviews in Mineralogy. **12,** pp. 644.

Rushmer T. (1991) Partial melting of two amphibolites: contrasting experimental results under fluid absent conditions. *Contrib. Mineral. Petrol.* **107,** 41–59.

Ryerson F. J. and Hess P. C. (1978) Implications of liquid-liquid distribution coefficients to mineral-liquid partitioning. *Geochim. Cosmochim. Acta.* **42,** 921–932.

Sawka W. N., Chappell B. W., and Norrish K. (1984) Light-rare-earth-element zoning in sphene and allanite during granitoid fractionation. *Geol.* **12,** 131–134.

Schmidt C., Chou I-M, Bodnar R. J., and Basset W. A. (1998) Microthermal analysis of synthetic fluid inclusions in the hydrothermal diamond anvil cell. *Am. Mineral.* **83,** 995–1007.

Schnetzler C. C. and Philpotts J. A. (1970) Partition coefficients of rare earth elements between igneous matrix material and rock-forming mineral phenocrysts-II. *Geochim. Cosmochim. Acta* **34,** 331–340.

Schreibber H. D., Lauer H. V., and Thanyasir T. (1980) The redox state of cerium in basaltic magmas: An experimental study of iron-cerium interactions in melts. *Geochim. Cosmochim. Acta* **44,** 1599–1612.

Shannon R. D. (1976) Revised effective ionic radii and systematic studies of interatomic distances in halides and chalcedonides. *Acta Cryst.* **A32,** 751–767.

Shaw D. M. (1970) Trace element fractionation during anatexis. *Geochim. Cosmochim. Acta* **34,** 237–243.

Shimizu N. (1998) The geochemistry of olivine-hosted melt inclusions in a FAMOUS basalt ALV519-4-1. *Phys. Earth Planet. Interiors* **107,** 183–201.

Shimizu N. and Hart S. (1982) Applications of the ion microprobe to geochemistry and cosmochemistry. *Ann. Rev. Earth Planet. Sci.* **10,** 483–526.

Shimizu N., Sobolev N. V., and Yefimova E. S. (1997) Chemical heterogeneities of inclusions in garnet and juvenile character of peridotitic diamonds from Siberia. *Russ. Geol. Geophys.* **38,** 356–372.

Skirius C. M., Peterson J. W., and Anderson Jr. A. T. (1990) Homogenizing rhyolitic glass inclusions from the Bishop Tuff. *Am. Mineral.* **75,** 1381–1398.

Sobolev A. V., Kamenetskiy V. S., Metrich N., Clochiatti R., Konokova N. N., Devirts A. L., and Ustinov V. I. (1990) Volatile regime and crystallization conditions in Etna Hawaiite lavas. *Geochem. Internat.* **1990,** 53–65.

Sobolev A. V., Migdisov A. A., and Portnyagin M. V. (1996) Incompatible element partitioning between clinopyroxene and basaltic liquid revealed by study of melt inclusions in minerals from Troodos Lavas, Cyprus. *Petrol.* **4,** 307–317.

Speer J. A. (1982) Zircon. *Orthosilicates* (ed. P. H. Ribbe), pp. 67–112. Mineral. Soc. America.

Student J. J. and Bodnar R. J. (1996) Melt inclusion microthermometry: petrologic constraints from the H_2O-saturated haplogranite system. *Petrol.* **4,** 310–325.

Student J. J. and Bodnar R. J. (1999) Synthetic Fluid Inclusions XIV: Coexisting silicate melt and aqueous fluid inclusions in the haplogranite-H_2O-NaCl-KCl system. *J. Petrol.* **40,** 1509–1525.

Thomas J. B. and Sinha A. K. (1999) Field, geochemical, and isotopic evidence for magma mixing and AFC processes in the Quottoon Igneous Complex, northwestern Br. Columbia and southeastern Alaska. *Can. J. Earth Sci.* **36,** 819–831.

Thomas R. (1994a) Estimation of viscosity and water content of silicate melts from melt inclusion data. *Eur. J. Min.* **6,** 511–535.

Thomas R. (1994b) Fluid evolution in relation to the emplacement of the Variscan granites in the Erzgebirge region: A review of the melt and fluid inclusion evidence. *Metallogeny of collisional orogens focussed on the Erzgebirge and comparable metallogenetic settings* (eds. R. Seltmann, H. Kampf, and P. Moller), pp. 70–81. Czech Geol. Surv..

Thomas R. and Webster J. D. (2000) Strong tin enrichment in a pegmatite-forming melt. *Mineral. Deposita.* **35,** 570–582.

Vityk M. O., Bodnar R. J., and Doukhan J. C. (2000) Synthetic fluid inclusions XV. TEM investigation of plastic flow associated with reequilibration of fluid inclusions in natural quartz. *Contrib. Mineral. Petrol.* **56,** 119–134.

Watson E. B. (1977) Partitioning of Mn between forsterite and silicate liquid. *Geochim. Cosmochim. Acta.* **41,** 1363–1374.

Watson E. B. (1980) Some experimentally determined zircon/liquid partition coefficients for the rare earth elements. *Geochim. Cosmochim. Acta.* **44,** 895–897.

Watson E. B. and Harrison T. M. (1983) Zircon saturation revisited: temperature and composition effects in a variety of crustal magma types. *Earth Planet. Sci. Lett.* **64,** 295–304.

Watson E. B., Sneeringer M. A., and Ross A. (1982) Diffusion of dissolved carbonate in magmas: experimental results and applications. *Earth Planet. Sci. Lett.* **61,** 346–358.

Webster J. D. and Rebbert C. R. (2001) The geochemical signature of fluid-saturated magma determined from silicate melt inclusions in Ascension Island granite xenoliths. *Geochim. Cosmochim. Acta.* **65,** 123–136.

Wolf M. B. and Wyllie P. J. (1994) Dehydration melting of amphibolite at 10 kb: the effects of temperature and time. *Contrib. Mineral. Petrol.* **115,** 369–383.

Wood B. J. and Blundy J. D. (1997) A predictive model for rare earth element partitioning between clinopyroxene and anhydrous silicate melt. *Contrib. Mineral. Petrol.* **129,** 166–181.

Yang K. and Bodnar R. J. (1994) Magmatic-hydrothermal evolution in the "Bottoms" of porphyry copper systems: evidence from silicate melt and aqueous fluid inclusions in granitoid intrusions in the Gyeongsang Basin, South Korea. *Int. Geol. Rev.* **36,** 608–628.